Strong-field ionization dynamics of a model H_2 molecule

Manfred Lein,[1] Thomas Kreibich,[2] E. K. U. Gross,[3] and Volker Engel[4]
[1]*Blackett Laboratory, Imperial College of Science, Technology and Medicine, London SW7 2BW, United Kingdom*
[2]*Institut für Theoretische Physik, Am Hubland, D-97074 Würzburg, Germany*
[3]*Institut für Theoretische Physik, Freie Universität Berlin, Arnimallee 14, D-14195 Berlin, Germany*
[4]*Institut für Physikalische Chemie, Am Hubland, D-97074 Würzburg, Germany*
(Received 28 August 2001; published 1 February 2002)

We investigate the dynamics of a one-dimensional H_2 model molecule in strong laser fields by numerical integration of the time-dependent Schrödinger equation without the use of the Born–Oppenheimer approximation. Ionization typically occurs at internuclear separations close to the ground-state equilibrium distance. This is contrary to the case of H_2^+, which ionizes at larger internuclear distances where charge-resonance-enhanced ionization is possible. Similar to the case of atoms, we find considerable nonsequential double ionization.

DOI: 10.1103/PhysRevA.65.033403 PACS number(s): 33.80.Rv, 31.70.Hq

I. INTRODUCTION

The dynamics of molecules under the influence of intense lasers displays a rich variety of interesting effects. We encounter not only the typical strong-field effects known from atoms: above-threshold ionization [1,2], harmonic generation [3–5], and nonsequential double ionization [6,7]. The additional degrees of freedom associated with the nuclear motion give rise to other phenomena such as above-threshold dissociation [8,9], bond softening [8,9], bond hardening [10], and charge-resonance-enhanced ionization (CREI) [11,12]. In spite of the steadily increasing computing capacities, an exact quantum-mechanical calculation for a molecule in a strong laser field has not been achieved yet. However, Chelkowski *et al.* managed to numerically solve the Schrödinger equation for H_2^+ driven by a strong field, with the only restriction being that the molecular axis is aligned with the laser polarization, but within a full treatment of the three-dimensional (3D) electronic motion [13]. All other approaches used additional approximations such as the Born-Oppenheimer (BO) approximation [14–16], reduced dimensionality for the electrons [17–19], or the single-active-electron (SAE) approximation [20]. A detailed comparison revealed pronounced differences between the BO and non-BO strong-field dynamics of H_2^+ in one dimension [19].

In this paper, we calculate the exact strong-field dynamics of a one-dimensional H_2 molecule, without adopting the BO or SAE approximation. We are, thus, able to study the interplay between vibrational motion and single or double ionization. For a molecular system with more than one electron, this is the first non-BO simulation of strong-field ionization. It is an extension of our previous work on harmonic generation by H_2 and HD model molecules [21] where non-BO effects have proven to be very important.

Using the BO approach, it was argued [22] that H_2 exhibits CREI, i.e., the ionization probability is strongly enhanced at internuclear distances much larger than the equilibrium distance. However, only a non-BO calculation can clarify if these distances are actually probed by the molecule after starting out from the molecular ground state. A further motivation for our study is the question whether nonsequential double ionization exists and, if so, whether it is governed by the same mechanism as found for atoms where rescattering appears to be the essential process [23–30]. Nonsequential ionization of atoms has been studied extensively, but for molecules it has received attention only in the last few years [31–34]. Experimentally, direct double ionization of H_2 has not been observed [35–37]. As we show below, however, it does clearly appear in our model calculations. We show that nonsequential double ionization provides an alternative explanation of experimental results [37] which have been ascribed to ionization of H_2^+ from its vibrational ground state.

II. MODEL

A direct numerical integration of the full time-dependent Schrödinger equation for the H_2 molecule in 3D is still not within reach. In order to be able to investigate the correlated electron-nuclear dynamics of this system, we employ a simplified model of the H_2 molecule where the motion of all particles is restricted to one spatial dimension. For linearly polarized fields, this can be justified by the observation that the dynamics of the charged particles predominantly follows the applied laser fields. Reduced dimensionality was first proposed to describe the interaction of a hydrogen atom with high-intensity laser pulses [38]. Since then, it has been shown that this model qualitatively reproduces all important strong-field effects such as multiphoton ionization, above-threshold ionization, or high-harmonic generation [39–41]. Moreover, it has provided valuable information in the investigation of electron correlation effects [29,42,43], which are responsible for the much-debated nonsequential double ionization yields of the He atom [6,7]. Likewise, the idea of reduced dimensionality was applied to the H_2^+ molecule [17,18]. As for the atoms, the model system reproduces all salient features of strong-field molecular dynamics. In particular, the typical interplay between the electronic and the nuclear motion is observed. Yet, due to the simplifications involved, the numerical effort is moderate.

In the following, we apply the idea of reduced dimensionality to the H_2 molecule. Since we will be concerned with radiation sources in the regime where the dipole approximation holds true, the center-of-mass (c.m.) motion of the molecule can be separated off. Then, considering linearly polarized external fields, the most important coordinates are the internuclear separation R and the electronic coordinates z_1

and z_2 in the direction of the laser polarization axis, measured with respect to the nuclear c.m. In terms of these coordinates, the model Hamiltonian reads (employing atomic units throughout this paper)

$$\hat{H}(t) = -\frac{1}{M}\frac{\partial^2}{\partial R^2} + \frac{1}{R} + W_{\mathrm{ee}}(z_1 - z_2) + \sum_{j=1}^{2}\left(-\frac{1}{2\mu_{\mathrm{e}}}\frac{\partial^2}{\partial z_j^2} + W_{\mathrm{en}}(z_j, R) + z_j E(t)\right), \quad (1)$$

where M is the proton mass, $\mu_{\mathrm{e}} = 2M/(2M+1)$ denotes the electronic reduced mass, and nondiagonal mass-polarization terms are neglected. The electron-electron repulsion and the electron-nuclear interaction are represented by soft-Coulomb potentials,

$$W_{\mathrm{ee}}(z_1 - z_2) = \frac{1}{\sqrt{(z_1 - z_2)^2 + \epsilon}}, \quad (2)$$

$$W_{\mathrm{en}}(z, R) = -\frac{1}{\sqrt{(z - R/2)^2 + \epsilon}} - \frac{1}{\sqrt{(z + R/2)^2 + \epsilon}}, \quad (3)$$

i.e., the Coulomb singularity is removed by introducing a smoothing parameter ϵ chosen equal to 1 unless stated otherwise. The laser field is represented in the length-gauge form in Eq. (1) where $E(t) = E_0 f(t)\sin(\omega t)$ denotes the electric field with peak amplitude E_0, envelope function $f(t)$, and laser frequency ω.

III. NUMERICAL CONSIDERATIONS

Employing the model Hamiltonian (1), the numerical solution of the corresponding time-dependent Schrödinger equation is obtained by means of the split-operator (SPO) technique [44]. However, when applied to molecular systems, the usual SPO technique does not take any advantage of the different time scales that govern the electronic and nuclear dynamics, respectively. Therefore, the original SPO scheme is slightly modified to allow for the use of different time steps in the propagation of the nuclear and electronic degrees of freedom, respectively.

Explicitly, the time-evolution operator propagating the total wave function by one time step Δt is approximated by

$$\exp(-i\hat{H}\Delta t) \approx \exp\left(-i\hat{T}_{\mathrm{n}}\frac{\Delta t}{2}\right)\{\hat{U}_{\mathrm{e}}^{\mathrm{SPO}}(\Delta t/N)\}^N \times \exp\left(-i\hat{T}_{\mathrm{n}}\frac{\Delta t}{2}\right), \quad (4)$$

where

$$\hat{U}_{\mathrm{e}}^{\mathrm{SPO}}(\Delta t) := \exp\left(-i\hat{T}_{\mathrm{e}}\frac{\Delta t}{2}\right)\exp(-i\hat{W}\Delta t) \times \exp\left(-i\hat{T}_{\mathrm{e}}\frac{\Delta t}{2}\right) \quad (5)$$

represents the electronic part of the evolution operator, $\hat{T}_{\mathrm{n}}$ and $\hat{T}_{\mathrm{e}}$ denote the nuclear and electronic kinetic-energy operators, respectively, and $\hat{W}$ subsumes all interactions and external potentials of the Hamiltonian, Eq. (1). According to Eq. (4), the electronic part described by the terms in curly brackets, is propagated N times by a smaller time step $\Delta t/N$, while the nuclear degrees of freedom are advanced only once by the larger time increment Δt. Evidently, since the nuclei move much slower than the electrons, $\hat{T}_n$ may be applied less frequently. An estimate for the upper limit of N can be obtained from considering the leading error terms introduced by the SPO method. Hardly surprising, for time-independent Hamiltonians, one finds that N can be of order $\mu_{\mathrm{n}}/\mu_{\mathrm{e}}$ without introducing additional errors compared to the ordinary SPO scheme. Of course, for an explicitly time-dependent Hamiltonian such as in Eq. (1), one has to ensure that Δt is small enough to resolve the nuclear motions and that $\Delta t/N$ allows for a proper description of the electronic dynamics. Typically, we found that $N \sim 25$ leads to an accurate integration of the time-dependent Schrödinger equation, including non-BO processes. Employing this parameter, the numerical effort can be reduced by almost a factor of 2 compared to the original SPO scheme. (Since even larger N reduce the computing time only marginally, no attempt was made to further optimize this quantity.)

The presented scheme is implemented by representing the wave function $\Psi(R, z_1, z_2, t)$ on a three-dimensional grid. The grid parameters are chosen such that the strong-field dynamics is properly represented on the grid. In particular, the grid spacings have to be small enough to resolve the typical momenta involved, e.g., the maximum classical electronic momentum $p_{\mathrm{max},e}^{\mathrm{class}} = E_0/\omega$. Typically, we found that grid spacing of $\Delta_R = 0.1$ a.u. and $\Delta_z = 0.4$ a.u., a time step of $\Delta t/N = 0.05$ a.u., and total grid sizes of $R_{\mathrm{max}} = 19$ a.u. and $\pm z_{\mathrm{max}} = 40$ a.u. provide sufficient convergence while leaving the computational effort manageable. We also mention that outgoing flux is absorbed by means of a mask function [45], so that spurious reflections from the grid boundaries are avoided.

IV. RESULTS AND DISCUSSION

Before the laser field is turned on, the molecule is assumed to be in its ground state, which is obtained by propagating the Schrödinger equation in imaginary time. From the exact symmetric ground-state wave function, we found an equilibrium separation of $\langle R \rangle = 2.2$ a.u. and the ground-state energy is $E_0 = -1.385$ a.u. corresponding to a dissociation energy of $D_0 = 0.0454$ a.u. (1.24 eV). For comparison we mention that the values for the real H_2 molecule are $\langle R \rangle = 1.4$ a.u., $E_0 = -1.16$ a.u., and $D_0 = 0.16$ a.u. (4.48 eV).

There is a considerable difference in the dissociation energy between 1D and 3D. One might, therefore, expect that the 1D molecule tends to dissociate more easily than the 3D molecule. Below, however, we will see that already in the 1D case, the dynamics takes place near the ground-state geometry and dissociation is negligible. Therefore, in this respect

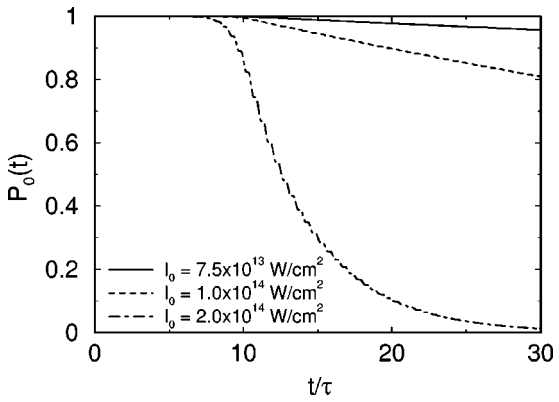

FIG. 1. Time evolution (in units of the laser cycle τ) of the norm $P_0(t)$, Eq. (6), for the model H_2 molecule in a $\lambda = 770$-nm laser field of various peak intensities I_0.

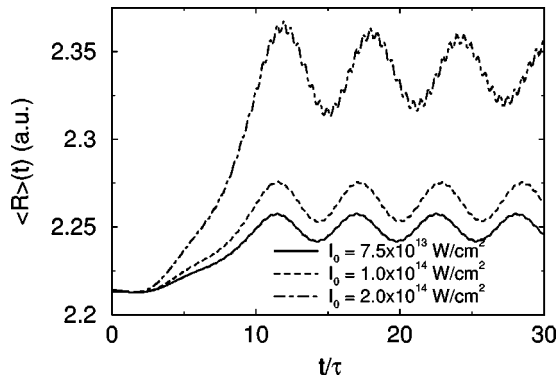

FIG. 2. Time evolution (in units of the laser cycle τ) of the mean internuclear distance $\langle R\rangle(t)$, Eq. (8), for the model H_2 molecule in a $\lambda = 770$-nm laser field of various peak intensities I_0.

we do not expect a large difference between the 1D and 3D dynamics.

We have first calculated the dynamics of the H_2 molecule in a laser field with $\lambda = 770$ nm for peak intensities of 7.5×10^{13} W/cm^2, 1×10^{14} W/cm^2, and 2×10^{14} W/cm^2. The envelope function $f(t)$ is chosen such that the field is linearly ramped from zero to the maximal field strength over the first 10 optical cycles τ and kept constant for another 20 τ. As mentioned above, the outgoing flux is absorbed by means of a mask function. Thus, the total probability remaining on the grid becomes time dependent:

$$P_0(t) := \int_{\text{grid}} dR dz_1 dz_2 |\Psi(R,z_1,z_2,t)|^2. \tag{6}$$

This quantity is associated with the probability of finding a still intact molecule at time t. For the chosen laser parameters, Fig. 1 shows the evolution of the time-dependent norm $P_0(t)$. Once the laser intensity is strong enough, the molecule starts to disintegrate. Hardly surprising, the decay probability increases with the peak laser intensity. Furthermore, after the laser pulse has been ramped to its maximum, i.e., after $t_1 = 10\,\tau$, we find an exponential decrease of the norm. Correspondingly, a decay rate Γ is defined according to

$$P_0(t - t_1) = e^{-\Gamma(t-t_1)}, \quad t \geqslant t_1. \tag{7}$$

By fitting the numerical curves for $P_0(t)$ to Eq. (7) in the constant-intensity interval, we obtain the decay rates given in Table I.

Employing the clamped-nuclei approximation, the ionization rates of the (one-dimensional) H_2 molecule were found to be strongly dependent on the internuclear separation [14]. Yet, the decrease of the norm observed in Fig. 1 is perfectly reproduced by a single decay rate. It seems that the radiation field did not substantially alter the internuclear separation during the propagation time for the laser parameters considered here. To further investigate this point, we have calculated the time-dependent expectation value of R,

$$\langle R\rangle(t) = \frac{\int_{\text{grid}} dR dz_1 dz_2 R|\Psi(R,z_1,z_2,t)|^2}{\int_{\text{grid}} dR dz_1 dz_2 |\Psi(R,z_1,z_2,t)|^2}. \tag{8}$$

As shown in Fig. 2, the molecule initially stretches and then starts to oscillate. By increasing the intensity, the amplitude and the period of the oscillations are increased, too. However, even for the highest intensity considered here, i.e., $I_0 = 2\times10^{14}$ W/cm^2, no signature of dissociation is found in the time evolution of $\langle R\rangle(t)$. This leads to the conclusion that the molecule predominantly decays due to ionization. Furthermore, the results show that, in the range of laser parameters considered here, the ionization rates near the equilibrium geometry dominate the dynamics—in sharp contrast to the situation found for the H_2^+ molecule [13]. We will see below that single ionization via multiphoton absorption is the primary mechanism, while (nonsequential) double ionization is weaker. Hence, the results provide clear evidence for the intermediate formation of H_2^+ molecular ions—in agreement with the experimental findings [8]. We mention in passing that the simulation does not further follow the dynamics of the produced H_2^+ molecules, since the corresponding part of the wave function is absorbed by the mask function.

In the following, we study the intensity dependence of single and double ionization for realistic laser pulses. We use 790-nm pulses with a $\sin^2$-shaped envelope function $f(t)$. The total duration of the pulses is chosen to be 28 optical cycles, corresponding to a full width at half maximum of 27 fs in intensity. When one of the electrons reaches the absorbing grid boundary we assume ionization. Now, the position of the other electron distinguishes between single and double ionization: For $|z| < 8$ a.u. we assume single ionization, oth-

TABLE I. Ionization rates Γ for the model H_2 molecule in a $\lambda = 770$ nm laser field.

I_0 (W/cm^2)	Γ (s^{-1})
7.5×10^{13}	8.6×10^{11}
1×10^{14}	4.0×10^{12}
2×10^{14}	8.3×10^{13}

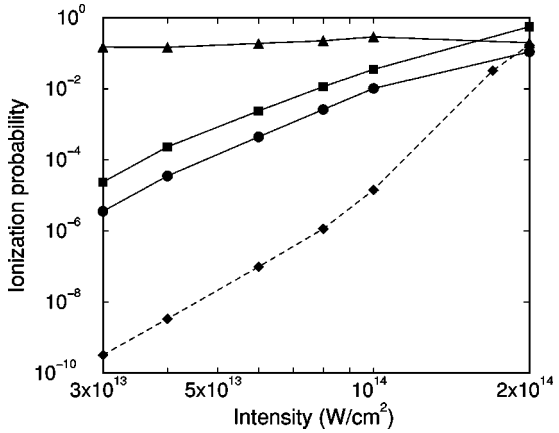

FIG. 3. Probabilities of single ionization (squares) and double ionization (circles) vs laser intensity for the model H_2 molecule in 790-nm pulses. Triangles: Ratio of double to single ionization. Diamonds: Ionization probability for the 1D H_2^+ molecular ion.

erwise double ionization. We integrate the loss at the grid boundaries over time to obtain the total probabilities for single and double ionization, $P^{(1)}$ and $P^{(2)}$. In a similar manner, the dissociation probability can be calculated. However, we find that dissociation into neutral fragments is always by orders of magnitude less likely than single or double ionization. The total propagation time is 32 optical cycles, i.e., the pulse duration plus four additional cycles. Within this time, practically all parts of the wave function corresponding to ionization reach the grid boundary so that the probabilities for single and double ionization are converged. The grid size along the electronic coordinates is always larger than four times the classical electronic oscillation amplitude $\alpha = E_0/\omega^2$. This means that possible rescattering processes are fully included.

Figure 3 shows the single- and double-ionization yield in the intensity range from 3×10^{13} W/cm^2 to 2×10^{14} W/cm^2. Also shown is the ratio between double and single ionization and the ionization probability of the one-dimensional H_2^+ molecular ion from its ground state. We observe that the ratio double to single ionization is typically several orders of magnitude larger than the ionization probability of H_2^+. This indicates clearly that double ionization is nonsequential in the intensity range under investigation. Here, ''nonsequential'' means that the double-ionization probability cannot be obtained as the product of the H_2 single-ionization probability and the H_2^+ ionization probability. Note that due to the absorbing boundary, our simulation does not include the process that an H_2^+ molecular ion—created by ionization of H_2—expands towards larger internuclear distances where enhanced ionization is possible. Rather, the strong double-ionization signal must stem from an almost simultaneous ejection of both electrons, see below for more detail.

At the highest intensity, the single-ionization probability is 56%, i.e., the onset of saturation in the single–ionization curve will be just above 2×10^{14} W/cm^2. In experiments on atoms [6,7] and molecules [31–33], a ''knee structure'' occurs in the intensity dependence of the double-ionization yield at about the same intensity where single ionization saturates. Consequently, if there is such a knee structure in the present case, then it must be outside the intensity range of Fig. 3. We note that the ratio double to single ionization is much less dependent on the intensity than the ionization probabilities themselves and varies around 0.2.

At this point, we mention that the calculated ionization probabilities depend on the smoothing parameter ϵ. However, we have found that the ratio between double and single ionization depends only slightly on ϵ. For example, choosing $\epsilon=1.44$ (corresponding to a ground-state energy of -1.174 a.u. which is very close to the 3D value -1.16 a.u.) gives a ratio of 0.21 at the intensity 8×10^{13} W/cm^2 compared to 0.23 for $\epsilon=1$.

To gain further insight into the double-ionization mechanism, we show in Figs. 4(a–e) and 5(a–e) snapshots of the two-electron configuration-space distribution,

$$\Gamma_{ee}(z_1,z_2,t)=\int dR|\Psi(R,z_1,z_2,t)|^2 \tag{9}$$

for the intensity 2×10^{14} W/cm^2. The snapshots are taken at times close to midpulse and are separated by time intervals of 0.05τ, where τ is the duration of an optical cycle. On the scale shown in Fig. 4, the ground-state distribution resides in a very small region around the origin. The density located along the axes corresponds to single ionization because there one electron is close to the nuclei while the other is far away from the nuclei. The density in the region where both electron coordinates have large absolute values corresponds to double ionization. The pictures are very similar to those obtained previously for the 1D helium model atom (see, e.g., Ref. [46]): In the double-ionization process, either both electrons emerge on opposite sides in patterns parallel to the axes (second and fourth quadrant), see Fig. 4, or they are ejected in the form of jets on the same side of the nuclei (first and third quadrant), see Fig. 5. This indicates that double ionization of H_2 proceeds in a similar manner as for He. The nonsequential ionization of atoms has been a much debated subject. According to the current knowledge [24–30], it is most likely caused by rescattering, i.e., after initial single ionization, one electron transfers energy to the second electron in a recollision event.

In the investigation of the double-ionization mechanism in atoms, the measurement and calculation of correlated electron-momentum spectra has played an important role [26,29]. We, therefore, proceed to study the electron-momentum distributions in the H_2 model molecule. Since it would be very demanding to calculate the final double-ionization spectra, we restrict ourselves to snapshots of the momentum distribution, taken during the time evolution under the influence of the laser pulse. These snapshots give us information about the final momentum spectrum if we keep in mind that a ponderomotive momentum shift has to be added to momentum values obtained from snapshots. The ponderomotive shift depends on the phase of the oscillating electric field at the time when the snapshot is taken [24–26]: If the field is at a local maximum or minimum, the ponderomotive shift is zero; if the field is zero, the momentum of

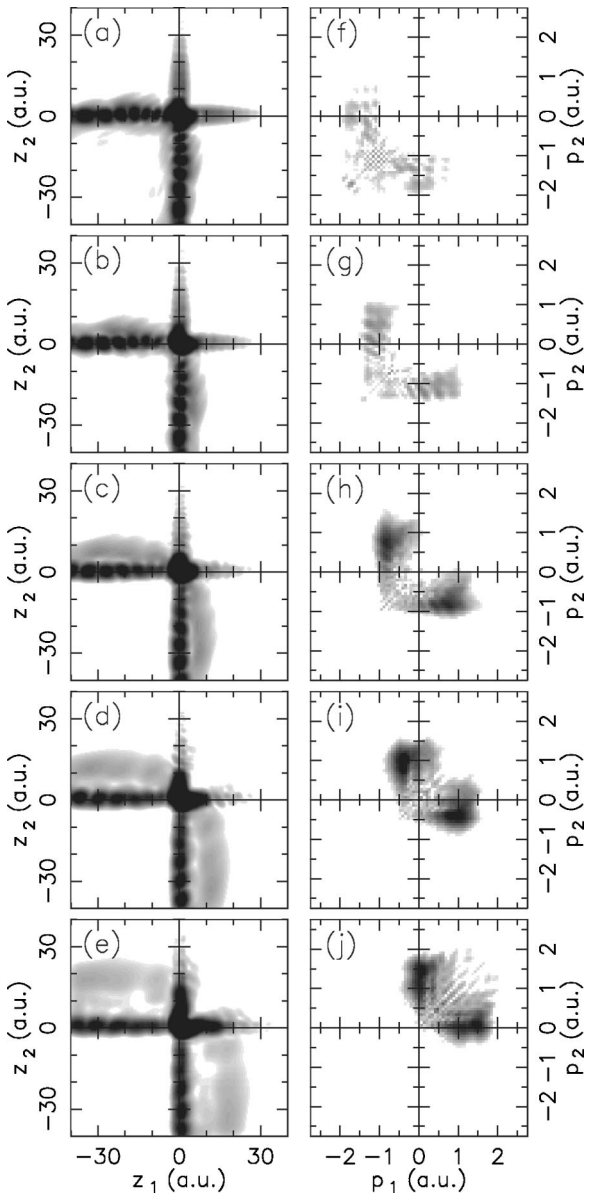

FIG. 4. Left: Snapshots of the two-electron density $\Gamma_{ee}(z_1,z_2,t)$, Eq. (9), for 1D H_2 in a 790-nm laser pulse with intensity 2×10^{14} W/cm^2, taken at the times (a) $t=13.55\tau$, (b) $t=13.6\tau$, (c) $t=13.65\tau$, (d) $t=13.7\tau$, and (e) $t=13.75\tau$. Right: Snapshots of the two-electron momentum distribution for the doubly ionized part of the wave function, taken at the same times. A logarithmic gray scale is employed.

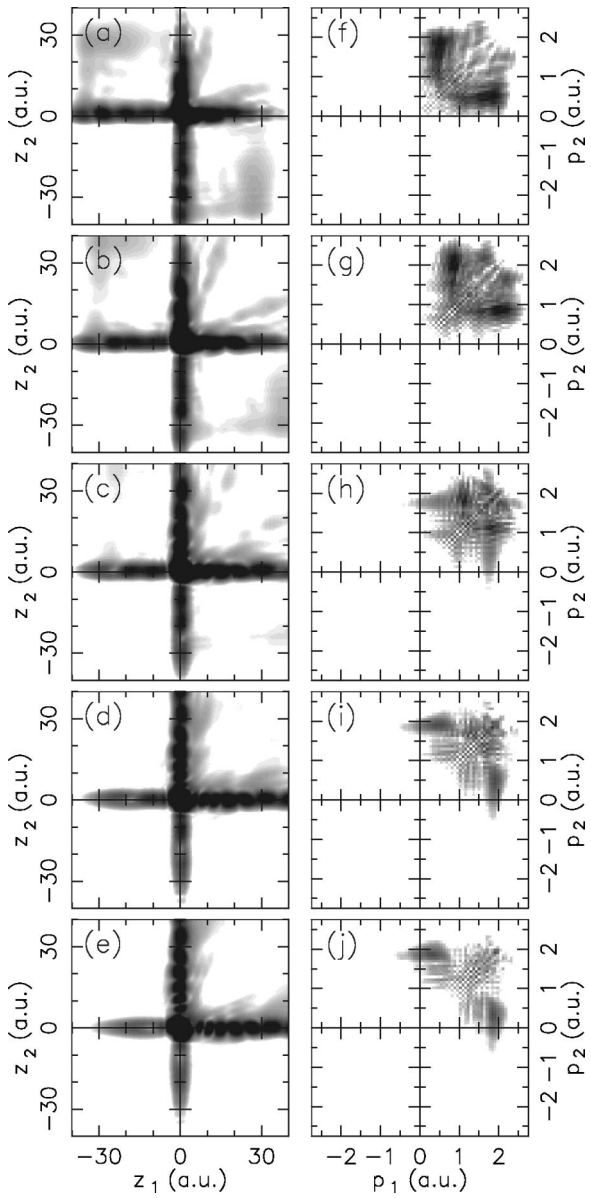

FIG. 5. Left: Snapshots of the two-electron density $\Gamma_{ee}(z_1,z_2,t)$, Eq. (9), for 1D H_2 in a 790-nm laser pulse with intensity 2×10^{14} W/cm^2, taken at the times (a) $t=13.8\tau$, (b) $t=13.85\tau$, (c) $t=13.9\tau$, (d) $t=13.95\tau$, and (e) $t=14\tau$. Right: Snapshots of the two-electron momentum distribution for the doubly ionized part of the wave function, taken at the same times. Same gray scale as in Fig. 4.

each electron is shifted by $\pm E_0/\omega$, corresponding to the acceleration within a quarter optical cycle.

Figs. 4(f–j) and 5(f–j) show momentum-distribution snapshots of the outer spatial regions that we define by $|z_1|$, $|z_2|>8$ a.u.. We find that the double ionization in Fig. 4 evolves to a stage [panels (e), (j)] where one electron is almost at rest, but nevertheless with a tendency that both electrons move into the same direction. This configuration will effectively receive no additional ponderomotive momentum shift during the remainder of the pulse since the electric field is at a local minimum in Figs. 4(e) and 4(j). This means that the momentum distribution in Fig. 4(j) can be viewed as the final momentum distribution for this process.

In almost all double ionization of Fig. 5, the electrons are initially ejected with momenta pointing in the same direction. However, the momenta will suffer an additional shift between zero and $-E_0/\omega$ per electron, where the value $-E_0/\omega=-1.3$ a.u. is for electrons ejected at $t=14\,\tau$ (zero electric field). Therefore, the final distribution will partly contain electrons moving in opposite directions.

The ionization of molecules, especially molecular ions, can be greatly enhanced at internuclear distances larger than the equilibrium distance [11,12]. This phenomenon has been termed CREI and can be visualized in the following way:

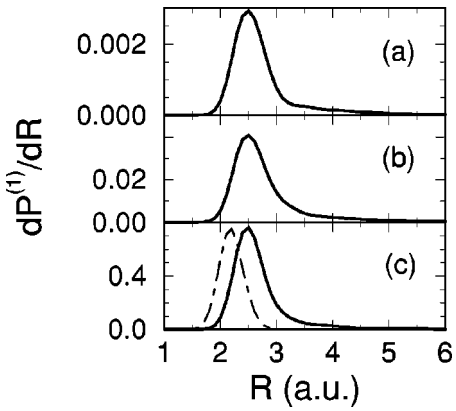

FIG. 6. *R*-dependent differential single-ionization probability for 1D H_2 in 790-nm pulses with intensities (a) 6×10^{13} W/cm^2, (b) 1×10^{14} W/cm^2, (c) 2×10^{14} W/cm^2 (solid curves). The dot-dashed curve in panel (c) is the ground-state nuclear density in arb. units.

The valence electrons move in a double-well potential created by the nuclei. In a laser pulse, the potential is periodically distorted by the electric field and an electron can temporarily get trapped in the upper well [12]. For certain internuclear distances, the internal potential barrier between the two wells is low and narrow so that tunneling of an electron through the barrier is very effective, leading to a large ionization rate.

Calculations with fixed internuclear distance *R* have been performed for one-dimensional H_2 [14] and three-dimensional H_2 [22], showing a strong enhancement of ionization at internuclear separations typically in the range from $R=3$ a.u. to $R=10$ a.u. Whether the molecule actually probes such large separations has remained an open question. In fact, it has usually been assumed that multiphoton ionization of H_2 occurs at the equilibrium geometry before the molecule has the chance to expand towards larger internuclear distances, see [36,47], and references therein. To settle this question, we analyze the numerical single-ionization probability $P^{(1)}$ into contributions from different values of *R*,

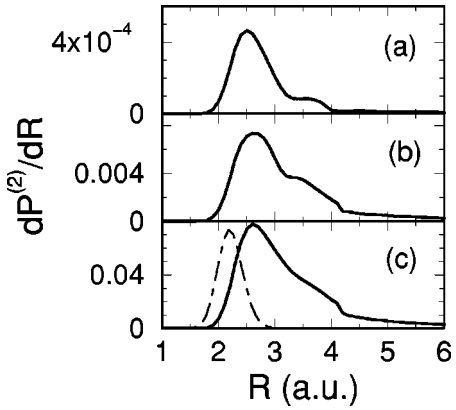

FIG. 7. *R*-dependent differential double-ionization probability for 1D H_2 in 790-nm pulses with intensities as in Fig. 6. The dot-dashed curve in panel (c) is the ground-state nuclear density in arb. units.

i.e., we calculate the differential probability $dP^{(1)}/dR$, see Fig. 6. The distribution turns out to be almost independent of the laser intensity. (This is also true for intensities not shown in Fig. 6.) It is a single peak with its maximum at $R=2.5$ a.u. The peak is located only slightly above the equilibrium distance $R_0=2.2$ a.u. For comparison, the nuclear density in the unperturbed ground state is shown in panel (g).

For double ionization, the *R*-dependent yield is given in Fig. 7. These distributions extend to somewhat larger *R*, and the maxima are located at slightly increased values of *R* as compared to single ionization.

For the highest intensity we have plotted snapshots of the two-body density

$$\Gamma_{\mathrm{ne}}(R,z,t)=2\int dz'\,|\Psi(R,z,z',t)|^2 \qquad (10)$$

in Fig. 8. For each internuclear separation *R*, this quantity gives the electron density as a function of *z*. The snapshots

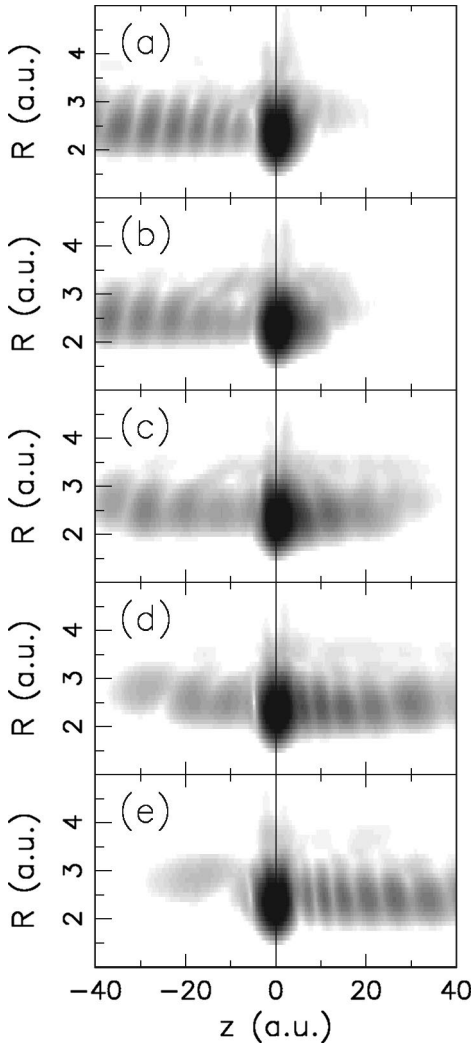

FIG. 8. Snapshots of the two-body density $\Gamma_{\mathrm{ne}}(R,z)$, Eq. (10), for the intensity 2×10^{14} W/cm^2 taken at (a) $t=13.6\tau$, (b) $t=13.7\tau$, (c) $t=13.8\tau$, (d) $t=13.9\tau$, and (e) $t=14\tau$. A logarithmic gray scale is employed.

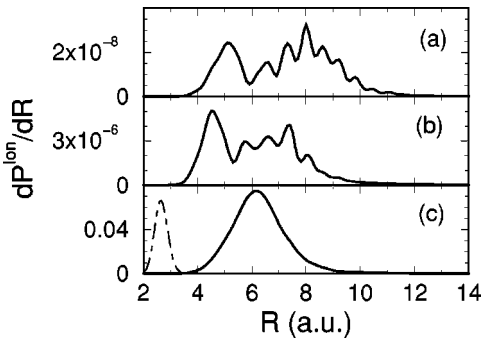

FIG. 9. *R*-dependent differential ionization probability for 1D H_2^+ in 790-nm pulses with intensities as in Fig. 6 (solid curves). The dot-dashed curve in panel (c) is the ground-state nuclear density of 1D H_2^+ in arb. units.

are taken during a half cycle with negative electric field so that we can trace the emission of an electron in positive *z* direction. Obviously, the electron is ejected at nuclear configurations close to the equilibrium position. It is also apparent that there is only a small change in *R* during the time between the ejection of an electron from the core region and its detection at the grid boundary. For example, in the right-hand side of panel (e), the lower end of the density distribution is always at $R \approx 1.8$ a.u., independently of the electron coordinate *z*. In addition, we find density at larger *R*, see, e.g., in Fig. 8(b) around $z=15$ a.u.. This is probability for an electron that was ejected during an earlier half cycle and is now oscillating in the field. In this case, the nuclei have had time to separate from each other so that the density is found at slightly increased *R*.

The ionization of 1D H_2^+ from its ground state is very different, see Fig. 9 for a direct comparison. The molecular ion is ionized at distances much larger than the equilibrium distance 2.66 a.u. Except for the highest intensity, the probability distributions have several maxima. For all intensities, the distributions are located between $R=4$ a.u. and $R=10$ a.u. This is the range where the critical distances for enhanced ionization are expected. This means that in H_2^+, the ionization probability at the ground-state geometry is so small that the molecule first expands to distances of enhanced ionization.

Double ionization of H_2 near the equilibrium distance initiates Coulomb explosion and, thus, produces fast protons. For example, Coulomb explosion from the 3D equilibrium distance 1.4 a.u. would give protons with a kinetic energy of 9.7 eV. We note that in most experiments on H_2, such large proton energies have not been observed [35–37]. However, a small number of such protons has been detected in Ref. [48]. Furthermore, Ref. [37] has reported on the measurement of fragments with energies up to 8 eV. These large energies were ascribed to the ionization of H_2^+ from the vibrational ground state. In the light of the present results we propose an alternative explanation: High-energy protons are created by double ionization of H_2 at internuclear distances close to (however, not exactly at) the equilibrium distance. Coulomb explosion from a distance of only 0.4 a.u. above the equilibrium distance leads to 7.6-eV protons, which is compatible with the results of Ref. [37]. In our simulation, 0.4 a.u. is about the shift between the equilibrium distance and the maximum of the *R*-dependent double-ionization yield, see Fig. 7. We consider this process more likely than the one proposed in Ref. [37] since the ionization probability of H_2^+ at its equilibrium distance is very small (see Ref. [49] for a 3D calculation).

V. CONCLUSION

We have investigated the dynamics of a model H_2 molecule driven by strong laser fields without adopting the Born-Oppenheimer approximation. It was found that for constant intensity the decay of the molecule can be described by a single decay rate. The internuclear distance of the neutral molecule stays always close to the equilibrium distance. The results indicate that single ionization at short internuclear distances is the main route of decay. Double ionization is much stronger than expected in a sequential process, and the ratio of double to single ionization is essentially independent of the laser intensity. Snapshots of the time evolution indicate that the mechanism of double ionization is very similar to atomic double ionization. Our calculation does, however, not include the process that an intermediate H_2^+ expands towards large internuclear distances *R* where it is easily ionized completely. The single and double ionization found in our calculations always occur at small *R*. This means that the neutral molecule does not reach the range of charge-resonance-enhanced ionization where the ionization probability would be much larger. This is contrary to the behavior of H_2^+ which suffers practically no ionization at the equilibrium distance even if the evolution starts from the total ground state. Double ionization of H_2 at small internuclear distances is possibly responsible for high-energy protons observed in Coulomb-explosion experiments.

ACKNOWLEDGMENTS

We are thankful for the support by the Deutsche Forschungsgemeinschaft and the Fonds der Chemischen Industrie.

[1] P. Agostini, F. Fabre, G. Mainfray, G. Petite, and N.K. Rahman, Phys. Rev. Lett. **42**, 1127 (1979).

[2] J.H. Eberly, J. Javanainen, and K. Rzążewski, Phys. Rep. **204**, 331 (1991).

[3] A. McPherson, G. Gibson, H. Jara, U. Johann, T.S. Luk, I.A. McIntyre, K. Boyer, and C.K. Rhodes, J. Opt. Soc. Am. B **4**, 595 (1987).

[4] A. L'Huillier, K.J. Schafer, and K.C. Kulander, J. Phys. B **24**, 3315 (1991).

[5] P. Saliéres, A. L'Huillier, P. Antoine, and M. Lewenstein, Adv.

At., Mol., Opt. Phys. **41**, 83 (1999).
[6] D.N. Fittinghoff, P.R. Bolton, B. Chang, and K.C. Kulander, Phys. Rev. Lett. **69**, 2642 (1992).
[7] B. Walker, B. Sheehy, L.F. DiMauro, P. Agostini, K.J. Schafer, and K.C. Kulander, Phys. Rev. Lett. **73**, 1227 (1994).
[8] P.H. Bucksbaum, A. Zavriyev, H.G. Muller, and D.W. Schumacher, Phys. Rev. Lett. **64**, 1883 (1990).
[9] A. Zavriyev, P.H. Bucksbaum, H.G. Muller, and D.W. Schumacher, Phys. Rev. A **42**, 5500 (1990).
[10] L.J. Frasinski, J.H. Posthumus, J. Plumridge, K. Codling, P.F. Taday, and A.J. Langley, Phys. Rev. Lett. **83**, 3625 (1999).
[11] T. Zuo and A.D. Bandrauk, Phys. Rev. A **52**, R2511 (1995).
[12] T. Seideman, M.Y. Ivanov, and P.B. Corkum, Phys. Rev. Lett. **75**, 2819 (1995).
[13] S. Chelkowski, T. Zuo, O. Atabek, and A.D. Bandrauk, Phys. Rev. A **52**, 2977 (1995).
[14] H. Yu, T. Zuo, and A.D. Bandrauk, Phys. Rev. A **54**, 3290 (1996).
[15] S. Geltman, J. Phys. B **32**, 2309 (1999).
[16] J.T. Lin and T.F. Jiang, Phys. Rev. A **63**, 013408 (2000).
[17] K.C. Kulander, F.H. Mies, and K.J. Schafer, Phys. Rev. A **53**, 2562 (1996).
[18] S. Chelkowski, C. Foisy, and A.D. Bandrauk, Phys. Rev. A **57**, 1176 (1998).
[19] T.D.G. Walsh, F.A. Ilkov, S.L. Chin, F. Châteauneuf, T.T. Nguyen-Dang, S. Chelkowski, A.D. Bandrauk, and O. Atabek, Phys. Rev. A **58**, 3922 (1998).
[20] K. Codling, L.J. Frasinski, and P.A. Hatherly, J. Phys. B **22**, L321 (1989).
[21] Th. Kreibich, M. Lein, V. Engel, and E.K.U. Gross, Phys. Rev. Lett. **87**, 103901 (2001).
[22] A. Saenz, Phys. Rev. A **61**, 051402 (2000).
[23] P.B. Corkum, Phys. Rev. Lett. **71**, 1994 (1993).
[24] Th. Weber *et al.*, Phys. Rev. Lett. **84**, 443 (2000).
[25] R. Moshammer *et al.*, Phys. Rev. Lett. **84**, 447 (2000).
[26] Th. Weber *et al.*, Nature (London) **405**, 658 (2000).
[27] A. Becker and F.H.M. Faisal, Phys. Rev. Lett. **84**, 3546 (2000).
[28] R. Kopold, W. Becker, H. Rottke, and W. Sandner, Phys. Rev. Lett. **85**, 3781 (2000).
[29] M. Lein, E.K.U. Gross, and V. Engel, Phys. Rev. Lett. **85**, 4707 (2000).
[30] J. Chen, J. Liu, L.B. Fu, and W.M. Zheng, Phys. Rev. A **63**, 011404 (2000).
[31] A. Talebpour, S. Larochelle, and S.L. Chin, J. Phys. B **30**, L245 (1997).
[32] C. Cornaggia and Ph. Hering, Phys. Rev. A **62**, 023403 (2000).
[33] C. Guo, M. Li, J.P. Nibarger, and G.N. Gibson, Phys. Rev. A **58**, R4271 (1998).
[34] A. Pegarkov, E. Charron, and A. Suzor-Weiner, J. Phys. B **32**, L363 (1999).
[35] M.R. Thompson, M.K. Thomas, P.F. Taday, J.H. Posthumus, A.J. Langley, L.J. Frasinski, and K. Codling, J. Phys. B **30**, 5755 (1997).
[36] T.D.G. Walsh, F.A. Ilkov, and S.L. Chin, J. Phys. B **30**, 2167 (1997).
[37] C. Trump, H. Rottke, and W. Sandner, Phys. Rev. A **60**, 3924 (1999).
[38] J. Javanainen, J.H. Eberly, and Q. Su, Phys. Rev. A **38**, 3430 (1988).
[39] J.H. Eberly, Q. Su, and J. Javanainen, Phys. Rev. Lett. **62**, 881 (1989).
[40] Q. Su and J.H. Eberly, Phys. Rev. A **44**, 5997 (1991).
[41] U. Schwengelbeck and F.H.M. Faisal, Phys. Rev. A **50**, 632 (1994).
[42] D. Bauer, Phys. Rev. A **56**, 3028 (1997).
[43] D.G. Lappas and R. van Leeuwen, J. Phys. B **31**, L249 (1998).
[44] M.D. Feit, J.A. Fleck, Jr., and A. Steiger, J. Comput. Phys. **47**, 412 (1982).
[45] K.C. Kulander, Phys. Rev. A **35**, 445 (1987).
[46] S.L. Haan, N. Hoekema, S. Poniatowski, W.-C. Liu, and J.H. Eberly, Opt. Express **7**, 29 (2000).
[47] C. Trump, H. Rottke, and W. Sandner, Phys. Rev. A **59**, 2858 (1999).
[48] G.N. Gibson, M. Li, C. Guo, and J. Neira, Phys. Rev. Lett. **79**, 2022 (1997).
[49] S. Chelkowski, T. Zuo, and A.D. Bandrauk, Phys. Rev. A **46**, R5342 (1992).